Supplementary Information *for*:

Clumped methane isotopologues ($^{13}CH_3D$ and $^{12}CH_2D_2$) of natural samples measured by high-resolution mass spectrometer with improved pretreatment system

Contents:

1. Supplementary Text

Text S1: *Calculation process of δD, $\delta^{13}C$, $\Delta^{13}CH_3D$, and $\Delta^{12}CH_2D_2$*

First, determine the bulk isotope composition of working gas (wg). VPDB refers to Vienna Pee Dee Belemnite and VSMOW to Vienna Standard Mean Ocean Water. $\delta^{13}C_{VPDB}$ and δD_{SMOW} of working gas(ref) were measured by Delta V IRMS using a GC–Isolink and a gas-bench (Thermo Fisher) and are termed $\delta^{13}C_{ref}$ and $\delta D_{ref,}$ respectively:

$$\delta^{13}C_{ref} = -43.54‰$$
$$\delta D_{ref} = -162.20‰$$

where $^{13}R_{VPDB}$=0.0112372, $^{D}R_{VSMOW}$=0.00015576 (Hayes, 1982).
Thus,

$$^{13}R_{ref} = \left(\frac{\delta^{13}C_{ref}}{1000}+1\right)\times {}^{13}R_{VPDB}$$

$$^{D}R_{ref} = \left(\frac{\delta D_{ref}}{1000}+1\right)\times {}^{D}R_{VSMOW}$$

The high-resolution isotope ratio mass spectrometer (253 Ultra, Thermo Fisher Scientific, Germany) measurement was then performed to obtain the sample gas values relative to the laboratory wg：$\delta^{13}C_{wg}$ and δD_{wg}:

$$^{12}CH_3D(frag)R_{sample} = \left(\frac{\delta D_{wg}}{1000}+1\right)\times {}^{D}R_{ref} \times 4 \,/\, 1+F\times 3\times {}^{D}R_{ref}$$

$$^{13}CH_4(frag)R_{sample} = \left(\frac{\delta^{13}C_{wg}}{1000}+1\right)\times {}^{13}R_{ref} \,/\, 1+F\times({}^{13}R_{ref}+3\times {}^{D}R_{ref})$$

And also, based on (Stolper et al., 2014 , Eldridge et al., 2019), the two can also be expressed as:

$$^{12}CH_3D(frag)R_{sample} = \frac{4\,{}^{D}R_{sample}}{1+3\times F\times {}^{D}R_{sample}}$$

$$^{13}CH_4(frag)R_{sample} = \frac{{}^{13}R_{sample}}{1+F\times({}^{13}R_{sample}+3\,{}^{D}R_{sample})}$$

An iterative calculation performed using *MATLAB*, yields $^{D}R_{sample}$ and $^{13}R_{sample:}$

$$^{D}R_{sample} = {}^{12}CH_3D(frag)R_{sample} \,/(4 -3\times F\times {}^{12}CH_3D(frag)R_{sample})$$

$$^{13}R_{sample} = {}^{13}CH_4(frag)R_{sample} \times (1+3\times F\times {}^{D}R_{sample}) \,/(1-F\times {}^{13}CH_4(frag)R_{sample})$$

At this time, the actual value of the wg needs to be determined, and here our assignment to the wg determines the transformation of the reference frame.

If the value of wg is assumed to be 0 here, i.e., $\Delta^{13}CH_3D_{ref}=\Delta^{12}CH_2D_{2\ ref}=0$, then

the sample is subsequently converted to the working gas reference frame'.

If we determine the value of wg as the real value here, which was calculated by temperature scale, then the sample will be converted to the absolute 'thermodynamic reference frame' later. The process of determination for wg value is described in the main text.

$$\Delta^{13}CH_3D_{ref}=2.27‰$$

$$\Delta^{12}CH_2D_{2\ ref}=3.51‰$$

The value of the reference gas relative to the random distribution is expressed as ${}^{13}CH_3DR_{ref\text{-}stoch}$ and ${}^{12}CH_2D_2R_{ref\text{-}stoch}$;

$${}^{13}CH_3DR_{ref\text{-}stoch}=4\times{}^{13}R_{ref}\times{}^{D}R_{ref}$$

$${}^{12}CH_2D_2R_{ref\text{-}stoch}=6\times{}^{D}R_{ref}\times{}^{D}R_{ref}$$

Therefore, the R-value under the ref frame is:

$${}^{13}CH_3DR_{ref}=\left(\frac{\Delta^{13}CH_3D_{\ ref}}{1000}+1\right)\times{}^{13}CH_3DR_{ref\text{-}stoch}$$

$${}^{12}CH_2D_2R_{ref}=\left(\frac{\Delta^{12}CH_2D_{2\ ref}}{1000}+1\right)\times{}^{12}CH_2D_2R_{ref\text{-}stoch}$$

Similarly, the spectrometer can measure the $\delta^{13}CH_3D_{wg}$ and $\delta^{12}CH_2D_{2\ wg}$ of the sample relative to the working gas and the R-value of the sample can be deduced as

$${}^{13}CH_3DR_{sample}=\frac{\left(\frac{\delta^{13}CH_3D_{wg}}{1000}+1\right)\times{}^{13}CH_3DR_{ref}}{1+F\times({}^{13}R_{ref}+3\times{}^{D}R_{ref})}\times[1+F\times({}^{13}R_{sample}+3\times{}^{D}R_{sample})]$$

$${}^{12}CH_2D_2R_{sample}=\frac{\left(\frac{\delta^{12}CH_2D_{2\ wg}}{1000}+1\right)\times{}^{12}CH_2D_2R_{ref}}{1+F\times({}^{13}R_{ref}+3\times{}^{D}R_{ref})}\times[1+F\times({}^{13}R_{sample}+3\times{}^{D}R_{sample})]$$

With these results, we can further calculate the final result:

$$\Delta^{13}CH_3D_{stoch}=[({}^{13}CH_3DR_{sample}/4\times{}^{13}R_{sample}\times{}^{D}R_{sample})-1]\times1000$$

$$\Delta^{12}CH_2D_{2\ stoch}=[({}^{12}CH_2D_2R_{sample}/6\times{}^{D}R_{sample}\times{}^{D}R_{sample})-1]\times1000$$

$$\delta D_{VSMOW}=\left(\frac{{}^{D}R_{sample}}{{}^{D}R_{VSMOW}}-1\right)\times1000$$

$$\delta^{13}C_{VPDB}=\left(\frac{{}^{13}R_{sample}}{{}^{13}R_{VPDB}}-1\right)\times1000$$

Text S2: *$\delta^{12}CH_2D_2$ Commissioning: Sensitivity or MRP ?*

The intensity of [$^{12}CH_2D_2^+$] on the spectrometer is generally very low due to the extraordinarily low abundance of $^{12}CH_2D_2$ (Zhang et al., 2021 , Stolper et al., 2014). Also, the [$^{12}CH_2D_2^+$] peak is located between the two adjacent adduct peaks of [$^{13}CH_5^+$] and [$^{12}CH_4D^+$] (Dong et al., 2020). This requires the measurement of $\Delta^{12}CH_2D_2$ to need a higher mass resolution power (MRP) and longer measurement time (which also means more sample volume) (Jautzy et al., 2021).

At the beginning of $\Delta^{12}CH_2D_2$ analysis, in November 2020, we assumed that maximizing MRP would be the priority objective. To this end the instrument was operated in HR mode and aperture was set to HR+.

Initially, the MRP was ~25,000, with ion source pressure below 2×10^{-7} mbar and the intensity of [$^{12}CH_2D_2^+$] was ~70cps **(Figure. S3 a)**. This performance is not able to resolve all the peaks of interest for methane clumped isotope analysis.

Improvement of MRP became a long-term goal and established the following operating procedures for the instrument. Accelerating Voltage (kV), Emission Control Current (mA), Trap Voltage (V), and other parameters are first stabilized. Extraction (%) and Electron Energy (V) are more related to adduct peak height, it is necessary to ensure that the impurity peak (e.g. [$^{13}CH_5^+$]) does not affect the target peak (e.g. [$^{12}CH_2D_2^+$]). X/Y Symmetry and Deflection (%) are more related to the overall intensity. When adjusting the ion source, ensure that the peak [$^{13}CH_5^+$] is lower than [$^{13}CH_3D^+$] and the target peak ([$^{12}CH_2D_2^+$]， [$^{12}CH_4^+$]) is as high as possible.

At this stage, ion optics tuning for resolution should be carried out. Focus and Rotation Quadrupole II (V) seem to be the most important variables that affect MRP. Additionally, we found during the commissioning process that water peaks may be more applicable to MRP commissioning (from Hao Xie, private communication). Theoretically, the water peak is consistent with the target peak, and the height of the water peak is higher and more sensitive to parameter changes. The parameters gain from water peak of MRP commissioning are also applicable to the target peak.

After ion source tuning and ion optics tuning commissioning, byApril 2021, the MRP reached 45,000-50,000, which can effectively separate the target peaks **(Figure. S3 b)**. However, the intensity of [$^{12}CH_2D_2^+$] is low (~55cps) and, small fluctuations lead to poor stability, and hence poor internal precision (±1 s.e.) $\delta^{12}CH_2D_2$ ~ ±2‰ that is not sufficiently precise for useful measurements.

Thus, we chose to make $\delta^{12}CH_2D_2$ measurement in HR mode facilitating enhanced signal intensity but requiring a peaking tailing correction procedure (Eldridge et al., 2019). The compromise MRP was ~ 30,000, with [$^{12}CH_4^+$] intensity (L4) of about 1.6 $\times$ 10^9 cps and [$^{12}CH_2D_2^+$] (H4 CDD) signal of ~ 120 cps **(Figure. 1d)** which gives an internal precision (±1 s.e. ~ ± 1.35 ‰) value which fulfills the measurement requirements.

Text S3: *Influence of temperature and humidity on magnetic field.*

In the $\delta^{12}CH_2D_2$ measurement configuration, with optimized sensitivity for H4CDD and a narrow entrance slit (HR mode, 5 μm), to ensure the stability of the [$^{12}CH_2D_2^+$] resolution, peak centering is based on [$^{13}CH_3D^+$] peak, and requires resolution of -0.004 to +0.0025 amu (ordinarily, the range was wider, but the peak height of [$^{13}CH_5^+$] may approach that of [$^{13}CH_3D^+$] with the narrowing of the slit or for biogenic-dominated environmental samples as shown in **Figure S4**), i.e., the offset of the magnetic field in one-$\delta^{12}CH_2D_2$ measurement-cycle should be less than this range.

During a period when the laboratory air-conditioning system was faulty, we found an offset of ~0.004 amu within 6 hours (**Figure S5**). Additionally, the frequent access of the experimenter also affected the stability of the magnetic field (the offset ~0.003 amu within 4 hours, the greater possibility here also was caused by ambient temperature and humidity changes). This offset is unrecognizable for peak centering procedure and will directly lead to the failure of the 16hrs $\delta^{12}CH_2D_2$ measurement. The optimized measurements require very fine peak centers, but this is only practical when the environment is stable enough and peak centers are not needed to compensate for changes in lab temperature. Under normal air-conditioning system operating parameters, the temperature change was ± 1°C, and the humidity change was ± 5% within 24hrs (**Figure S6a**) whereas with a faulty air-conditioning system, sudden temperature changes reached 5°C, and the change in humidity could reach more than 40% (**Figure S6b**).

In our experience, the effect of temperature and humidity on the spectrometer magnetic field may be delayed, so we monitor the results on a longer time scale. It has also been shown that CH_4 clumped isotope measurement can be carried out by maintaining temperature (± 1°C) and humidity (± 5%) stable over long periods of time.

Text S4: *Details of Gas Capillary Leaking Experiments.*

For our measurement, the key point is not the variation of one side of the reference gas in separate measurement cycles, because the reference cylinder gas (wg) is refilled for each sample, but we focus on the difference between samples, i.e., whether the results obtained with different inlet and compression ratios are consistent, and if different, whether dependence exists. In addition, one difference with the gas-leaking experiments of Yan et al. is that we use both sides of the gas (sample and reference) for simultaneous leaking, and 20 times compressions of 20%-100% of the bellows before each measurement to ensure uniform internal isotope distribution, to minimize any possible isotopic fractionation induced by diffusion (Stolper et al., 2014 , Young et al., 2017). The equilibrium intensity of the dual inlet is achieved by press adjusting, the tolerance intensities of both bellows sides to ~1% of the target level.

Here, only the results for δD are shown. For the other three indicators ($\delta^{13}C$, $\delta^{13}CH_3D$, and $\delta^{12}CH_2D_2$), on the one hand, the $\delta^{12}CH_2D_2$ measurement will consume about 50% of the total gas volume, in this process, the $\delta^{12}CH_2D_2$ internal accuracy (±1 s.e.) satisfied the analysis requirements showing the stability of $\delta^{12}CH_2D_2$ measurement. On the other hand, the gas volume and compression ratio used in each measurement of $\delta^{13}C$-$\delta^{13}CH_3D$ and $\delta^{12}CH_2D_2$ were different, but there was no significant difference in the results **(Table S1).**

In the mass spectrometer dual-inlet mode, it is easy to have inconsistent compression ratios on both bellow sides. In case of insufficient gas volume, a maximum compression difference of ~30% can be reached (e.g., 2022/5/1 results), and this difference is the first source that needs to be considered, potentially causing isotope fractionation. The gas sample volume in which the measurement was performed is the second possible influence, and the L1 intensity is a more visual indicator of the inlet volume, which varies from 2.29×10^8cps to 5.69×10^8cps to better compare the differences in the results **(Table 4)**.

The samples analyzed on 2022/4/24 did not experience repeated compression of the bellows (right sample bellow has a greater compression ratio than left reference bellow), the 50% consumption in the previous $\delta^{12}CH_2D_2$ measurement may have led to isotopic fractionation of the residual gas, the largest difference in this δD (wg) results is 0.24‰ **(Table 4)**, and the highest was from the 2022/4/24 measurement, the subsequent sample's δD(wg) appeared the isotopic slightly enrichment (-32.34‰) also seems acceptable.

Text S5: *Equilibrium Verification of Heating Experiments, Evidence from 500°C.*

The equilibrium state of methane isotopologues is the result of C-H bond activation and hydrogen isotope exchange. Performing heated gas equilibrium experiments requires exposing CH_4 exposed methane gas to the catalyst at high temperatures in the 300 – 500°C temperature interval. The key point of heating experiments is whether the sample gas reaches clumped isotope equilibrium by heating. Generally, the longer the heating time, the better clumped-isotopologues-equilibrium will be reached, but it is worth noting that there are decomposition reactions in the heating of methane (Asai et al., 2008), where the products are hydrogen and multi-walled carbon nanotubes, with higher temperatures being more favorable to the decomposition of methane. Stolper et al. found that ~1/2 of the starting methane converted to H_2 throughout heating experiments at 500 °C. We also found that the highest amount of hydrogen was produced after heating at 500 °C and relatively less after heating at 300 °C when purifying the heated gas samples. Furthermore, in this process, methane adsorption below 700°C was disturbed by surface hydrogen atoms (Asai et al., 2008) and methane conversion decreased with time due to carbon deposition as a by-product during the methane cracking reaction, which led to clogging of the active center and reduction of catalyst surface area (Abbas and Wan Daud, 2010 , Asai et al., 2008), which added uncertainty to the process of achieving methane clumped isotopic equilibrium by heating. It has been shown that heating methane gas with different δD values to 500 °C can verify the equilibrium of clumped isotopologues (Stolper et al., 2014 , Eldridge et al., 2019), and in this study, different duration times of heating at 500 °C were compared to verify the possible equilibrium interval.

The distribution of heating times at 500°C ranged from 1.5 h to 24 h, and the percentage of methane decomposition could reach up to ~50%. The heating duration times were chosen following the experimental protocols of Stolper et al., 2014, Eldrigethe et al., 2019 and Zhang et al., 2021. We believe that methane samples reach equilibrium within a few hours under the combined effect of nickel catalyst (65 wt.% nickel dispersed on a silica/alumina support; Sigma Aldrich) and heating at 500°C. Nonetheless, longer time intervals were considered to remain consistent with previous work. Our results showed that all samples (n=11) yielded external precision (±1 s.d.) for $\Delta^{13}CH_3D$ of ~ ±0.39‰ and $\Delta^{12}CH_2D_2$ of ~ ±1.35‰ **(Table S5)**, which can be considered generally acceptable. Additionally, the results obtained at 500°C were grouped with a 5-hour heating time as the limit, i.e., 1.5 ~ 6 hrs of heating as a short-heated duration group and 8 ~ 24 hrs of heating as a long-heated duration group. The differences between the two groups were compared and ANOVA was performed separately **(Table S6)**: For the two groups obtained by $\Delta^{13}CH_3D$, p-value ~ 0.96 > 0.05, there was no significant difference between the two groups; For the two groups obtained by $\Delta^{12}CH_2D_2$, p-value ~ 0.08 > 0.05, also show no significant difference between the two groups. Therefore, the effect of heating duration is negligible, and these results are statistically considered to have reached thermodynamic equilibrium.

2. Supplementary Table

Table S1. Results for house CH_4 standard (HL and JH). Uncertainties represent by internal precision (±1 s.e.) and external precision (±1s.d.).

Methane type	Pretreatment‡	Date	$\delta D_{(wg)}$	1 s.e.‰	1 s.d. ‰	$\delta^{13}C_{(wg)}$	1 s.e.‰	1 s.d. ‰	$\Delta^{13}CH_3D_{(wg)}$	1 s.e.‰	1 s.d. ‰	$\Delta^{12}CH_2D_{2(wg)}$	1 s.e.‰	1 s.d. ‰
Pure CH_4 (HL)	Cylinder gas	2021/8/26	0.11	0.05		0.00	0.01		0.09	0.35		-1.48	2.70	
	Cylinder gas	2021/8/31	0.00	0.05		0.00	0.01		-0.94	0.36		-0.97	2.22	
	Cylinder gas	2021/9/6	-0.04	0.04		0.01	0.00		-0.24	0.27		-0.71	1.56	
	Cylinder gas	2021/10/18	-0.09	0.04		0.00	0.01		0.08	0.31		1.05	1.30	
	Cylinder gas	2021/10/23	-0.01	0.08		0.01	0.01		-0.32	0.31		1.72	1.35	
	Cylinder gas	2021/10/25	-0.06	0.05		0.03	0.01		0.23	0.36		2.48	1.41	
	Cylinder gas	2021/10/27	0.01	0.05	0.07	-0.01	0.01	0.07	0.13	0.30	0.35	1.65	1.25	1.20
	Cylinder gas	2022/1/1	0.02	0.06		0.17	0.02		0.69	0.35		-0.71	1.45	
	Cylinder gas	2022/1/16	0.03	0.07		0.08	0.02		0.16	0.36		0.55	1.59	
	Cylinder gas	2022/1/20	0.01	0.07		0.12	0.02		-0.08	0.33		0.00	1.42	
	Cylinder gas	2022/2/22	-0.03	0.08		0.07	0.02		0.04	0.33		-1.08	1.68	
	Cylinder gas	2022/2/24	0.14	0.07		0.20	0.02		0.13	0.31		-0.40	1.52	
	Cylinder gas	2022/2/26	0.05	0.09		0.00	0.03		-0.29	0.34		-0.54	1.39	
	Cylinder gas	2022/3/1	-0.11	0.08		0.15	0.03		0.17	0.31		1.32	1.42	
	Direct collect	2021/9/13	0.22	0.05		-0.54	0.01		-0.03	0.28		0.09	1.77	
	Direct collect	2022/1/10	0.91	0.07		0.17	0.02		0.15	0.36		0.34	1.53	
	Direct collect	2022/1/14	1.09	0.06		0.55	0.02		0.03	0.33		-0.47	1.46	
	Direct collect	2022/1/18	0.89	0.07	0.24	0.13	0.02	0.43	-0.22	0.37	0.35	0.42	1.46	1.34
	Flame-seal	2022/3/5	0.62	0.08		-0.17	0.01		0.55	0.27		-0.49	1.35	
	Flame-seal	2022/3/7	0.52	0.07		-0.63	0.01		0.43	0.29		-0.67	1.37	
	Flame-seal	2022/3/9	0.49	0.07		-0.79	0.01		-0.26	0.29		2.29	1.42	
	45K-70K Direct collect	2022/3/11	0.65	0.08		0.04	0.01		0.26	0.29		-1.28	1.58	

	45K-70K Flame-seal	2022/1/22	0.78	0.08		0.41	0.02		0.65	0.36		-2.59	1.38	
	45K-70K Flame-seal	2022/3/3	0.80	0.08		-0.09	0.02		-0.42	0.33		1.98	1.50	
	45K-70K Flame-seal	2022/3/21	0.46	0.09		-0.62	0.01		0.58	0.34		1.04	1.42	
Pure CH_4 (JH)	Cylinder gas	2022/4/13	-32.58	0.08	0.06	8.06	0.01	0.01	0.01	0.38	0.09	0.53	1.51	0.49
	Cylinder gas	2022/4/24	-32.42	0.13		8.07	0.01		0.09	0.24		-0.69	1.44	
	Cylinder gas	2022/4/28	-32.55	0.07		8.05	0.01		0.22	0.25		0.00	1.32	
	Cylinder gas	2022/5/15	-32.55	0.05		8.06	0.01		-0.01	0.26		0.47	1.30	
	45K-70K Direct collect	2022/6/3	-31.68	0.07	0.25	8.21	0.01	0.26	0.42	0.30	0.23	0.61	1.36	0.54
	45K-70K Direct collect	2022/6/5	-31.20	0.07		8.67	0.01		-0.05	0.25		0.58	1.32	
	50K-75K Direct collect	2022/6/18	-31.24	0.08		8.56	0.01		-0.02	0.29		0.84	1.33	
	50K-75K Direct collect	2022/6/20	-31.80	0.08		8.08	0.01		0.29	0.29		-0.68	1.34	
	50K-75K Direct collect	2022/6/22	-31.67	0.08		8.01	0.01		0.52	0.30		0.57	1.22	

‡In addition to Cylinder gas representing the direct release of gas from the cylinder, to verify the fractionation of the pretreatment process, there are five different treatments here:

(1. Direct collection, using Kimble glass bottles filled with silica gel to collect the cylinder gas directly and release it after five minutes of heating;

(2. Flame-seal, using Pyrex break-seal tubes filled with silica gel and then flame-sealed;

(3. 45K-70K Direct collect, using a cryogenic vacuum line to purify cylinder gas at 45K and collect with Kimble glass bottles filled with silica gel at 70K;

(4. 50K-75K Direct collect, using a cryogenic vacuum line to purify cylinder gas at 50K and collect with Kimble glass bottles filled with silica gel at 75K;

(5. 45K-70K Flame-seal, purification at 45K using cryogenic vacuum line followed by collection at 70K with Pyrex break-seal tubes filled with silica gel.

* Isotope data reported in this table are referred to as 'working gas reference frame'. The working gas was assumed to have the following isotope signatures: $\delta^{13}C$=0‰; δD=0‰; $\Delta^{13}CH_3D$=0‰; $\Delta^{12}CH_2D_2$=0‰.

Table S2. Comparison of typical accuracy and precision as achieved in different Ultra HR-IRMS laboratories (University of California, Berkeley; Tokyo Institute of Technology; California Institute of Technology; Tianjin University).

		Shot noise limit	UC Berkeley	Tokyo Tech	Caltech	Tianjin University
Internal precision (1 s.e.)	$\delta^{13}C$	±0.01‰	±0.01‰	±0.01‰	±0.01‰	±0.01‰
	δD	±0.12‰	±0.12‰	±0.11‰	±0.12‰	±0.05‰
	$\delta^{13}CH_3D$	±0.28‰	±0.25‰	±0.35‰	±0.28‰	±0.29‰
	$\delta^{13}CH_2D_2$	±1.00‰	±1.35‰	±1.35‰	±1.10‰	±1.30‰
External precision (1 s.d.)	$\delta^{13}C$		±0.02‰	±0.03‰	±0.03‰	±0.03‰
	δD		±0.15‰	±0.09‰	±0.20‰	±0.10‰
	$\Delta^{13}CH_3D$		±0.25‰	±0.31‰	±0.35‰	±0.30‰
	$\Delta^{12}CH_2D_2$		±1.35‰	±1.24‰	±1.22‰	±1.34‰

Table S3. Results for pretreatment process fractionation.

	Direct collect CH_4 No purification			Flame-seal CH_4 No purification			Direct collect CH_4† Purified:45K purify and 70K collect			Flame-seal CH_4 Purified:45K purify and 70K collect			Direct collect CH_4† Purified: 50K purify and 75K collect			All processed samples		
	mean	1 s.d.	1 s.e.*	mean	1 s.d.	1 s.e.*	mean	1 s.d.	1 s.e.*	mean	1 s.d.	1 s.e.*	mean	1 s.d.	1 s.e.*	mean	1 s.d.	1 s.e.*
$\delta^{13}C_{(wg)}$	0.24	0.53	0.01	-0.53	0.26	0.01	0.27	0.25	0.01	-0.10	0.42	0.01	0.16	0.25	0.01	-0.02	0.43	0.01
$\delta D_{(wg)}$	0.27	0.17	0.08	0.54	0.06	0.09	0.94	0.28	0.07	0.68	0.16	0.10	0.96	0.24	0.08	0.78	0.29	0.09
$\Delta^{13}CH_3D_{(wg)}$	-0.02	0.14	0.34	0.24	0.36	0.30	0.16	0.20	0.30	0.27	0.49	0.36	0.18	0.22	0.28	0.16	0.32	0.33
$\Delta^{12}CH_2D_{2(wg)}$	0.40	0.23	1.38	0.38	1.35	1.50	-0.23	0.74	1.32	0.14	1.97	1.40	0.16	0.66	1.30	0.14	1.12	1.35
n	4			3			3			3			3			16		

†For statistical convenience, the JH gas results are unified in the HL gas framework (assuming consistent gases on both sides) for comparison.

*All s.e. values are reported as averages of s.e. values for several samples, which are not statistically meaningful but representative of the samples' measurement level.

Table S4 δD Results when changing the gas volume and bellow compression.

Data	Left bellow (sample gas)[a]		Right bellow (reference gas)[b]		Measurement volume[c]	L1 intensity(cps)	δD (wg, ‰)	1 s.e. (‰)
	Volume (mbar)	Compression (%)	Volume (mbar)	Compression (%)				
2022/4/24[d]	72	86	61	69	82	4.10E+08	-32.34	0.10
2022/4/25	53	62	37	32	82	4.12E+08	-32.49	0.13
2022/4/28	90	92	90	91	98	4.71E+08	-32.44	0.07
2022/4/30	35	49	25	27	68	3.34E+08	-32.50	0.05
2022/5/1	33	65	22	39	50	2.29E+08	-32.59	0.07
2022/5/15	104	100	104	100	104	5.69E+08	-32.55	0.05

[a] Initial sample gas volume (mbar) and bellow compression reading (%) of the left bellow. [b] Initial reference gas volume (mbar) and bellow compression reading (%) of the right below. [c] Represents the gas volume (mbar) to be measured after bellow compression. [d] Without repeated 20 times bellow compression from 20% to 100% for the 2022/4/24 sample.

Table S5. Theoretical predictions results comparison of *ab initio* and *PIMC.*

Temperature(℃)	*Ab initio* (Young et al., 2017)		PIMC (Eldrige et al., 2019)	
	$\Delta^{13}CH_3D$	$\Delta^{12}CH_2D_2$	$\Delta^{13}CH_3D$	$\Delta^{12}CH_2D_2$
0	6.6352	23.7097	6.6920	23.3589
50	5.0371	16.1958	5.1027	16.1348
100	3.9253	11.2905	3.9821	11.3829
150	3.1131	8.0301	3.1577	8.1894
200	2.4989	5.8262	2.5431	5.9996
250	2.0254	4.3075	2.0727	4.4705
300	1.6557	3.2402	1.7043	3.3852
350	1.3642	2.4757	1.4107	2.6034
400	1.1322	1.9183	1.1742	2.0329
450	0.9461	1.5051	0.9822	1.6117
500	0.7957	1.1943	0.8254	1.2975
550	0.6732	0.9574	0.6968	1.0610
600	0.5727	0.7745	0.5910	0.8815
650	0.4897	0.6319	0.5037	0.7444
700	0.4207	0.5194	0.4314	0.6391
750	0.3630	0.4300	0.3714	0.5578
800	0.3145	0.3583	0.3216	0.4947
850	0.2735	0.3004	0.2800	0.4457
900	0.2387	0.2533	0.2454	0.4074
950	0.2090	0.2147	0.2164	0.3775
1000	0.1835	0.1829	0.1921	0.3541
Correlation Analysis	P-value：0.000255; t Stat: 4.4823;			
ANOVA*	P-value：0.9566649; F：0.00299; F crit: 4.084			

*ANOVA is an abbreviation for "ANalysis Of VAriance".

Table S6. Summary of individual measurements from equilibrated methane experiments(n=19). Compositions are reported in units of permil (‰). Uncertainties represent by internal precision (±1 s.e.) and external precision (±1s.d.).

Data	T(℃)	Methane type	Duration(hr)	δD_{VSMOW}	1 s.e.	$\delta^{13}C_{VPDB}$	1 s.e.	$\Delta^{13}CH_3D$(wg)	$\Delta^{13}CH_3D$	1 s.e.	1 s.d.	$\Delta^{12}CH_2D_2$(wg)	$\Delta^{12}CH_2D_2$	1 s.e.	1 s.d.	tailing value
2022/5/28	500	JH	1.5	-194.65	0.07	-39.61	0.01	-1.44	0.82	0.34		-1.19	2.31	1.11		0.58
2022/6/7	500	HL	2	-185.13	0.07	-47.67	0.01	-1.89	0.38	0.30		-1.05	2.45	1.21		0.72
2022/5/30	500	JH	3	-194.80	0.09	-41.04	0.01	-1.06	1.21	0.27		-0.92	2.58	1.20		0.67
2022/1/12	500	HL	5	-188.73	0.07	-49.24	0.02	-0.84	1.42	0.32		-0.84	2.71	1.61		0.04
2022/5/11	500	JH	6	-204.76	0.08	-42.59	0.01	-1.43	0.84	0.27		-2.75	0.75	1.20		0.38
2022/4/26	500	HL	8	-203.25	0.08	-50.47	0.01	-1.66	0.61	0.36	0.39	-0.97	2.58	1.69	1.35	0.06
2022/4/30	500	HL	13	-187.16	0.10	-45.23	0.01	-1.00	1.27	0.24		-3.26	0.24	1.32		0.11
2022/5/18	500	JH	15	-196.73	0.07	-41.62	0.01	-0.94	1.33	0.35		-3.50	-0.01	1.10		0.33
2022/4/19	500	HL	18	-204.71	0.08	-50.03	0.01	-2.08	0.19	0.37		-0.94	2.57	1.54		0.97
2022/3/24	500	HL	21	-200.28	0.09	-50.15	0.01	-1.28	0.98	0.35		-3.53	0.00	1.50		2.32
2022/4/15	500	HL	24	-201.03	0.10	-50.25	0.01	-1.10	1.16	0.45		-4.72	-1.23	1.56		0.65
2022/3/15	400	HL	5	-202.01	0.07	-47.87	0.01	-1.51	0.75	0.30		-0.51	2.99	1.21		2.88
2022/5/2	400	HL	10	-198.54	0.05	-47.92	0.01	-0.79	1.48	0.30	0.34	-0.02	3.49	1.15	1.30	1.51
2022/6/1	400	JH	18	-202.28	0.08	-40.64	0.01	-1.45	0.82	0.26		-1.30	2.21	1.17		0.73
2022/3/17	400	HL	20	-201.15	0.09	-46.77	0.01	-0.80	1.47	0.33		-3.42	0.08	1.39		1.72
2022/5/4	300	HL	40	-201.38	0.07	-46.89	0.01	-0.53	1.74	0.27		-0.36	3.15	1.39		0.05
2022/5/13	300	HL	67	-199.15	0.09	-46.55	0.01	-0.60	1.67	0.26	0.08	-0.75	2.75	1.25	0.35	0.08
2022/5/9	300	HL	76	-206.71	0.07	-47.38	0.01	-0.75	1.52	0.27		0.23	3.74	0.97		0.70
2022/5/7	300	HL	90	-194.82	0.07	-47.04	0.01	-0.60	1.67	0.39		-0.34	3.17	1.22		0.18

* Isotope data reported in this table are referred to working gas. The working gas used in this study, the HL cylinder gas, has the following isotope signatures: $\delta^{13}C$(VPDB)=-45.16‰; δD(SMOW)=-162.81‰; $\Delta^{13}CH_3D$=2.27‰; $\Delta^{12}CH_2D_2$=3.51‰.

Table S7. Grouping of heating experiments at 500°C and ANOVA* results.

$\Delta^{13}CH_3D$ (wg, ‰)		$\Delta^{12}CH_2D_2$ (wg, ‰)	
Heated 1.5 ~6hrs	Heated 8 ~24hrs	Heated 1.5 ~6hrs	Heated 8 ~24hrs
-1.44	-1.66	-1.19	-0.97
-1.89	-1.00	-1.05	-3.26
-1.06	-0.94	-0.92	-3.50
-0.84	-2.08	-0.84	-0.94
-1.43	-1.28	-2.75	-3.53
p-value:0.96	-1.10	p-value:0.08	-4.72
F crit:5.11	F:0.002	F crit:5.11	F:3.72

*ANOVA is an abbreviation for "ANalysis Of VAriance".

3. Supplementary Figures

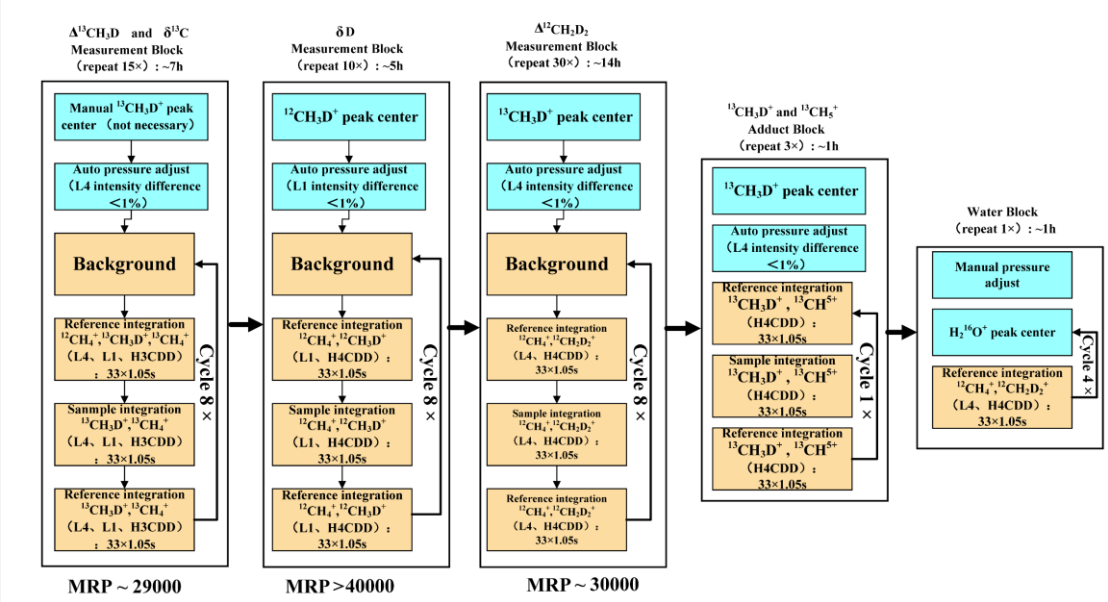

Figure. S1. Flow chart of CH_4 measurement. (a)$\Delta^{13}CH_3D$ and $\delta^{13}C$ analysis was carried out together in high resolution (HR) mode with a 5 μm entrance slit and the aperture was set to standard when MRP~29,000. The H3 CDD collector was used to record [$^{13}CH_3D^+$] intensity, and L4 and L1 received [$^{12}CH4^+$] and [$^{13}CH4^+$] at the same time. There were 8 cycles × 15 blocks in the procedure, the total time is about 7 hrs; (b) δD analysis was in HR+ mode (with 5 μm entrance slit and aperture set to HR+), and MRP reached 45,000 to 50,000 to make sure the [$^{12}CH_3D^+$] peak relatively flat. Faraday cup L1 recorded [$^{12}CH4^+$] intensity while H4 CDD recorded [$^{12}CH_3D^+$] intensity. 8 cycles × 10 blocks were included in the measurement procedure for about 7 hrs; (c)$\Delta^{12}CH_2D_2$ analysis was in HR mode while aperture was set to standard when MRP~30,000. The H4 CDD was used for [$^{12}CH_2D_2^+$] intensity while L4 for [$^{12}CH4^+$], (d)the tailing correction was carried out after the $\Delta^{12}CH_2D_2$ measurement (8 cycles × 30 blocks), the total duration of the two was about 14 hrs.

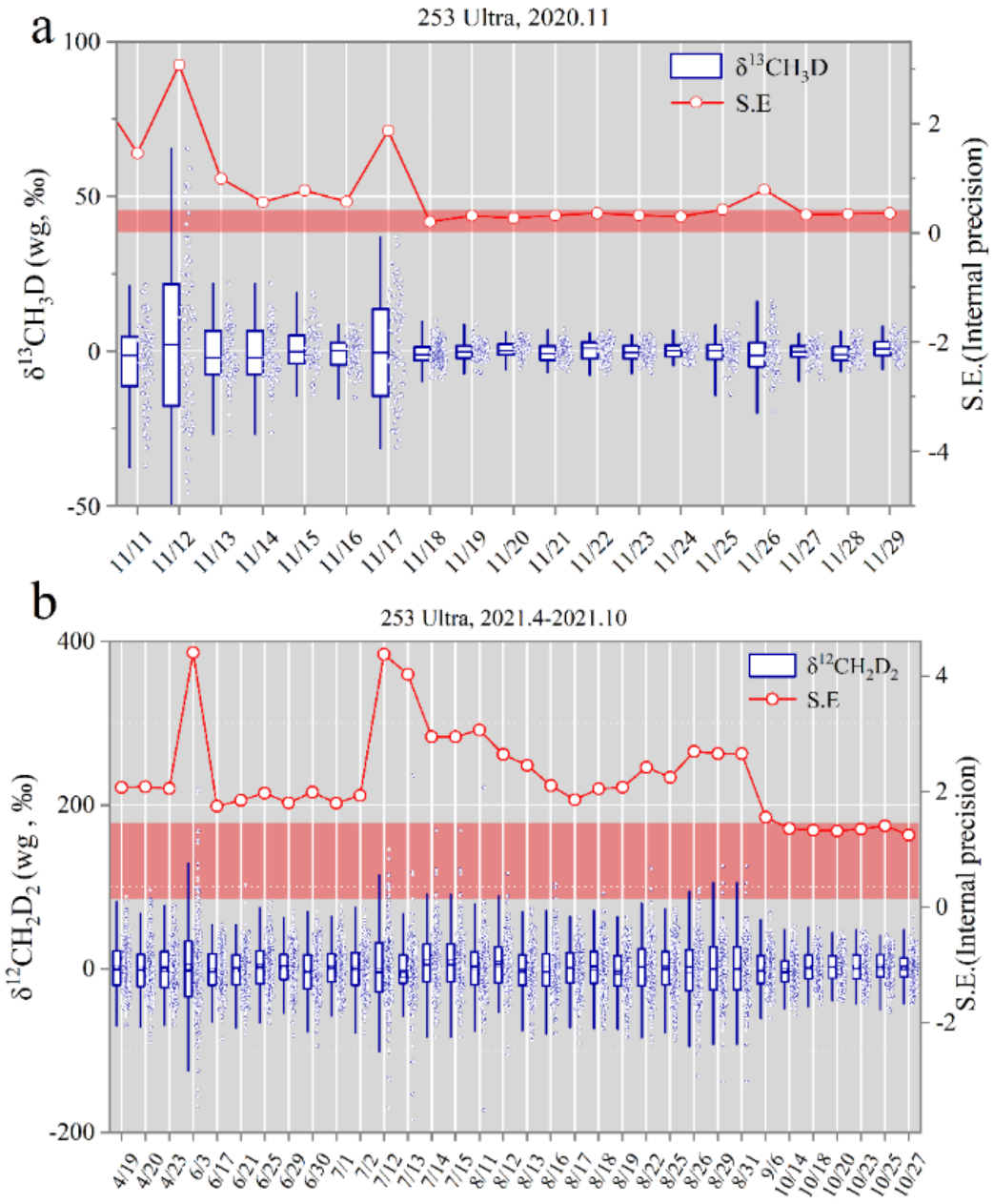

Figure. S2. The commissioning process for (a) $\delta^{13}CH_3D$ and (b) $\delta^{12}CH_2D_2$. The red shaded areas represent the internal accuracy (±1 s.e.) ranges of ±0.35‰ and ±1.35‰ for $\delta^{13}CH_3D$ and $\delta^{12}CH_2D_2$, respectively. The number of tests is $\delta^{13}CH_3D$ ~ 8 cycles × 15 blocks and $\delta^{12}CH_2D_2$ ~ 8 cycles × 30 blocks, respectively. The blue box plots show the 25th-75th percentile ranges of the test results for $\delta^{13}CH_3D$ (wg) and $\delta^{12}CH_2D_2$ (wg), with the squares representing the mean and the horizontal lines representing the median.

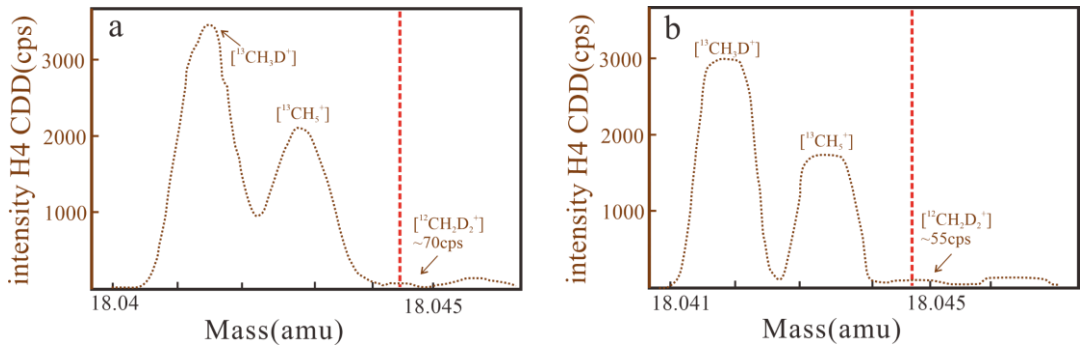

Figure. S3. Mass scans for [$^{12}CH_2D_2^+$] in HR+ mode, (a) in November 2020; (b) in April 2021. (cps = counts per second).

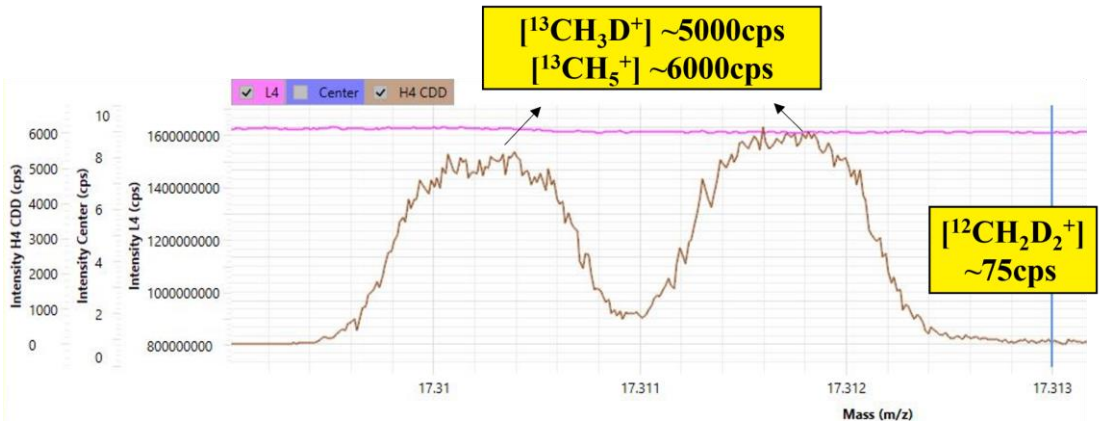

Figure. S4. [$^{12}CH_2D_2^+$] scan result of biogenic-dominated environmental sample (QingNian Lake).

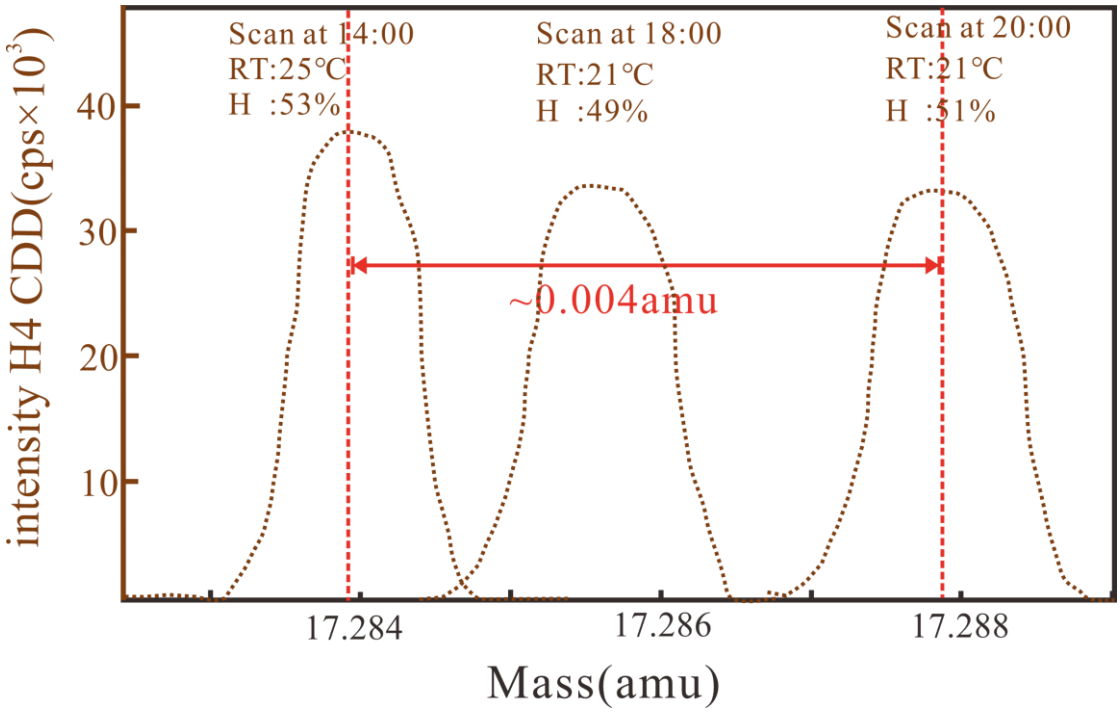

Figure. S5. Water scan result when the air-conditioning system is faulty on April 8, 2022. The left peak is the scan result at 2 p.m., the room temperature (RT) is 25℃ and

the humidity (H) is 53%; The right peak is the scan result at 8 p.m., the room temperature (RT) is 21℃ and the humidity (H) is 51%. The actual mass of the water peak should be 18.011. Water peak is the intensity of water [H_2O^+] from the H4 CDD. The mass displayed by the water peak scanning is different due to the change of the center position. (cps = counts per second).

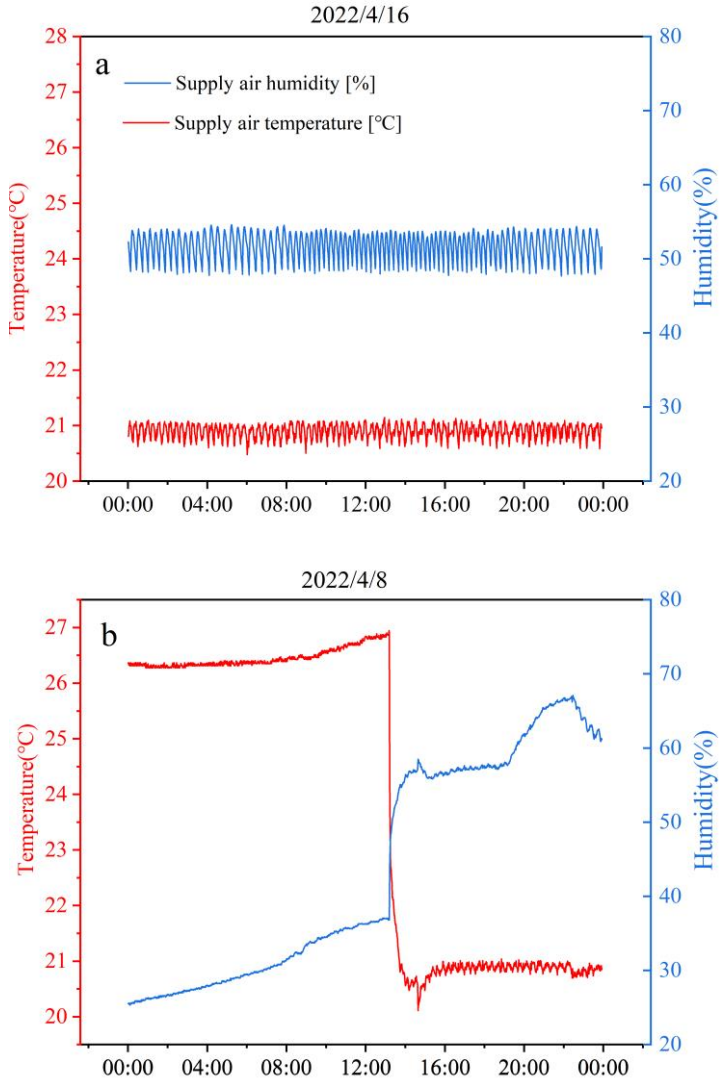

Figure. S6. Laboratory air-conditioning systems supply air temperature (AT) and humidity detection results. (a) is the case of the normal air-conditioning system, 2022/4/16; (b) is the case of air-conditioning system failure, 2022/4/8. The red line represents temperature, the blue line represents humidity, and the detection time is ten minutes apart, ranging from 0:00 to 24:00 on the day. We noted that the supply air temperature (AT) is different from the room temperature (RT), the change of AT is usually earlier than RT.

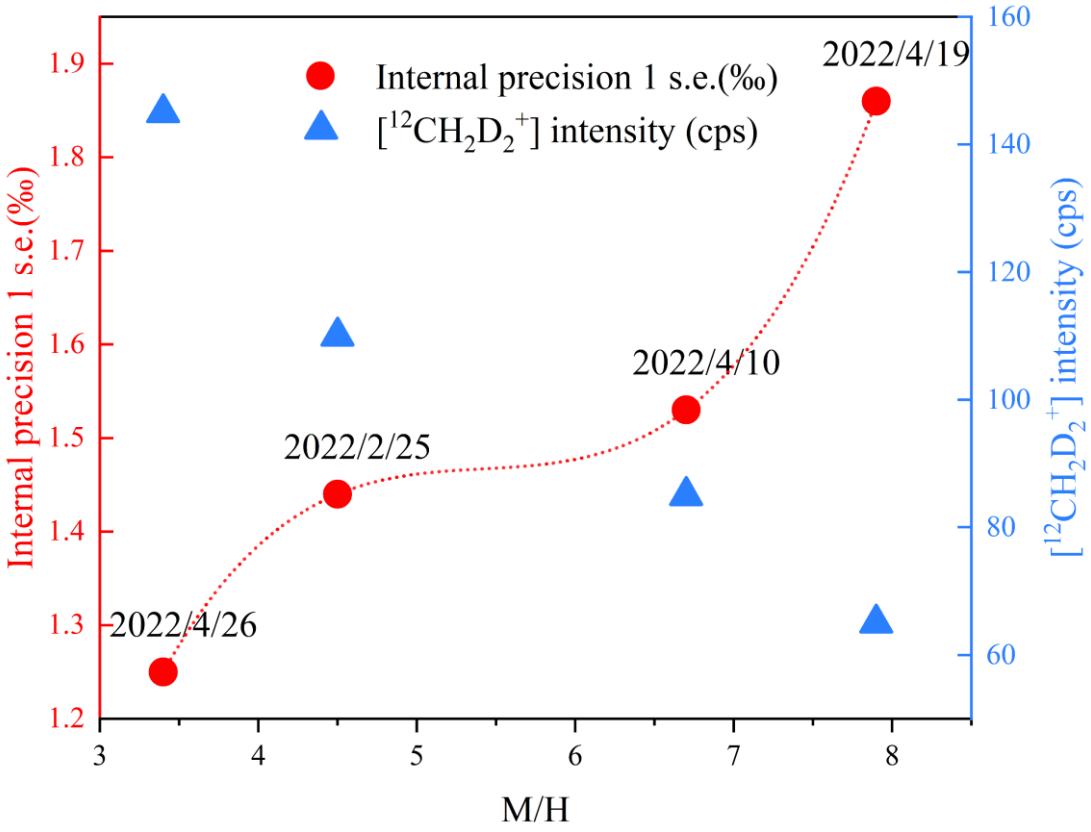

Figure. S7. Relationship of $\delta^{12}CH_2D_2$ analysis internal precision (1 s.e, ‰) / [$^{12}CH_2D_2^+$] intensity (cps) and slit quality (M/H). These results were done with similar gas volumes (source pressure) and the same measurement procedure ((8 cycles × 30 blocks, with tailing correction).

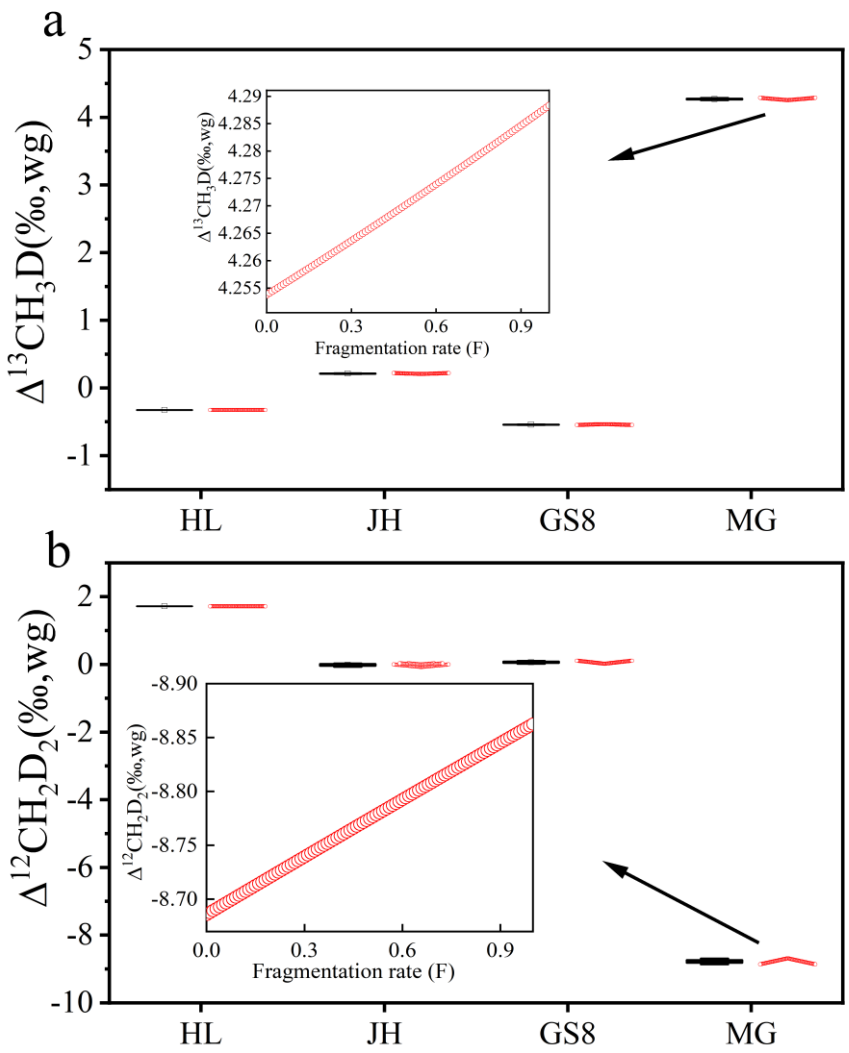

Figure. S8. (a) $\Delta^{13}CH_3D$ (wg) and (b) $\Delta^{12}CH_2D_2$ (wg) change. The black lines are a boxplot of the 25th-75th percentile of the data, the transparent box represents the mean value, and the red part represents the scatter distribution, the partially enlarged view shows that the MG $\Delta^{13}CH_3D$ and $\Delta^{12}CH_2D_2$ value changes via fragmentation rate (F) value from 0 to 1. HL and JH represent HaoLun and JinHong cylinder gas, GS8 is a natural gas sample and MG represents a kind of mixed gas.

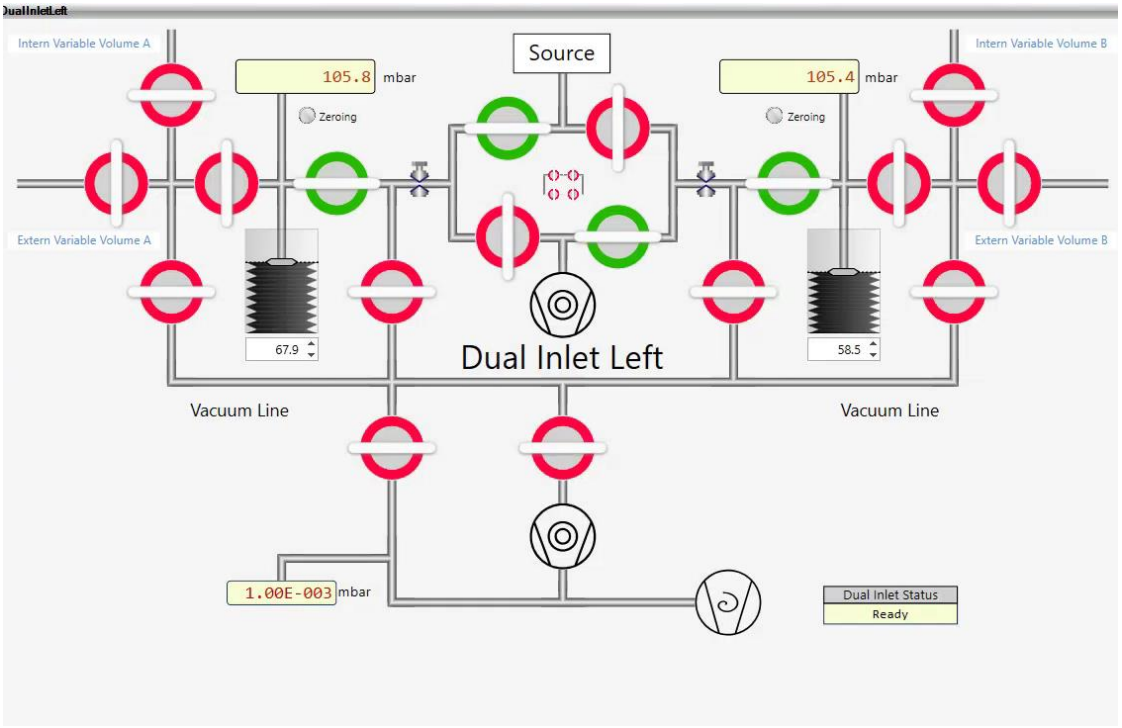

Figure. S9. Screenshot of the spectrometer dual-inlet system.

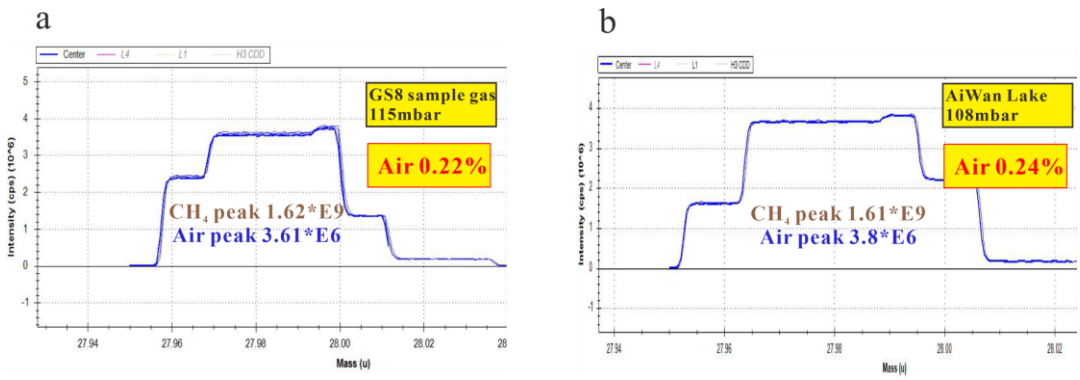

Figure. S10. Air scan result. (a) is GS8 sample gas; (b)is Aiwan Lake sample gas. CH_4 peak is the intensity of mass-16 [$^{12}CH_4^+$] from L4. Air peak is the intensity of mass-28 from the Center cup. For the purity of the samples, we used the intensity of mass-28 to compare the intensity of mass-16 to indicate the air content, compared the signal values of mass-16 of the purified samples and cylinder gas under the same pressure, and finally verified the purity of the purified samples obtained.

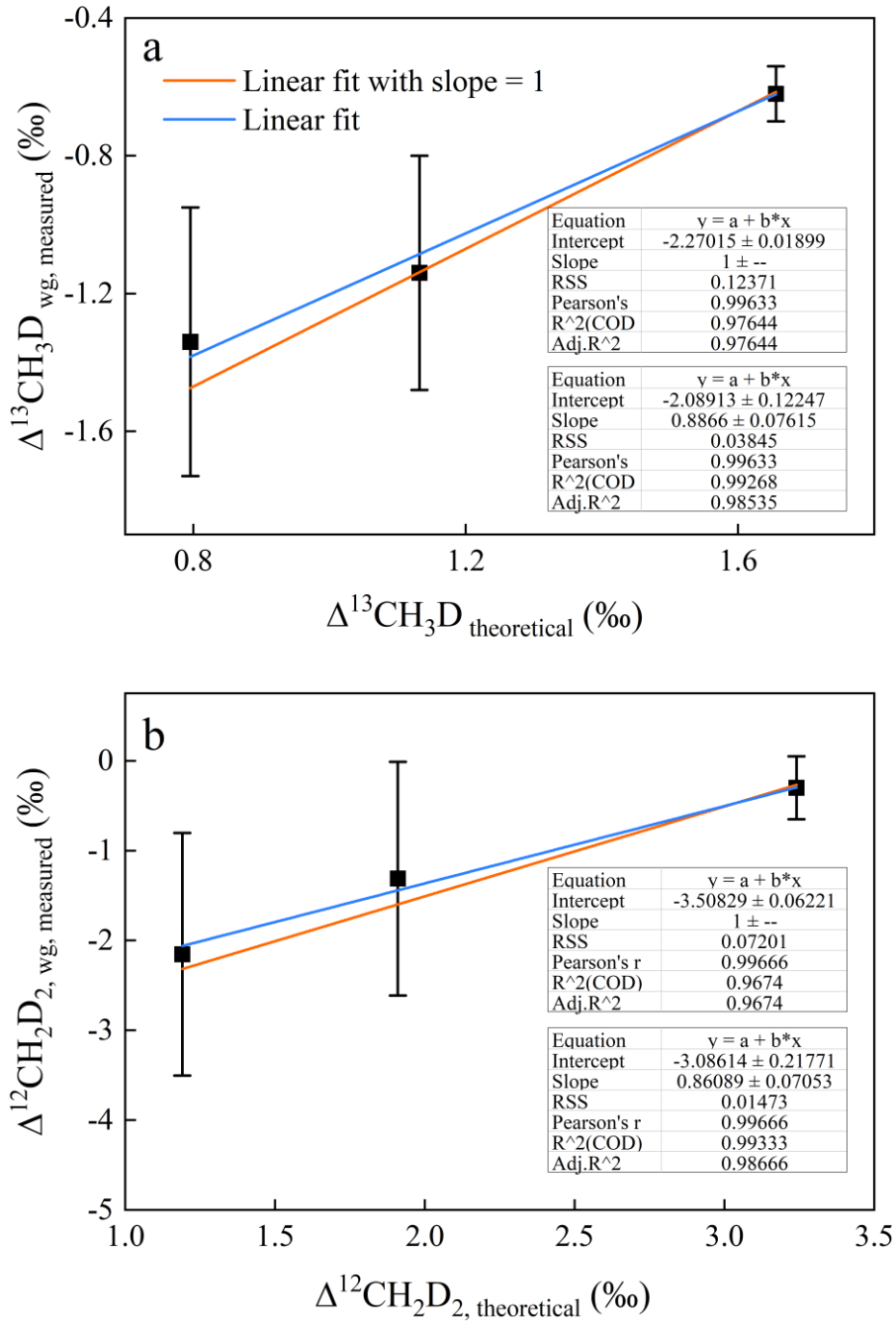

Figure.S11. Linear fitting result of heating experiments from 300–500 ℃. (a) is $\Delta^{13}CH_3D_{wg,measured}$ v.s. $\Delta^{13}CH_3D_{\ theoretical}$; and (b) is $\Delta^{12}CH_2D_{2,\ wg,measured}$ v.s. $\Delta^{12}CH_2D_{2,\ theoretical}$. The black blocks represent the average value in heating temperature (from left to right: 500℃, n=11 400℃, n =4; 300℃, n=4). Error bars represent the external precision (±1s.d.) among samples heating at the same temperature. RSS represents the residual sum of the square. Adj. R-Square represents the result of adjusting R-squared by the sample numbers n and the number of independent variables k.

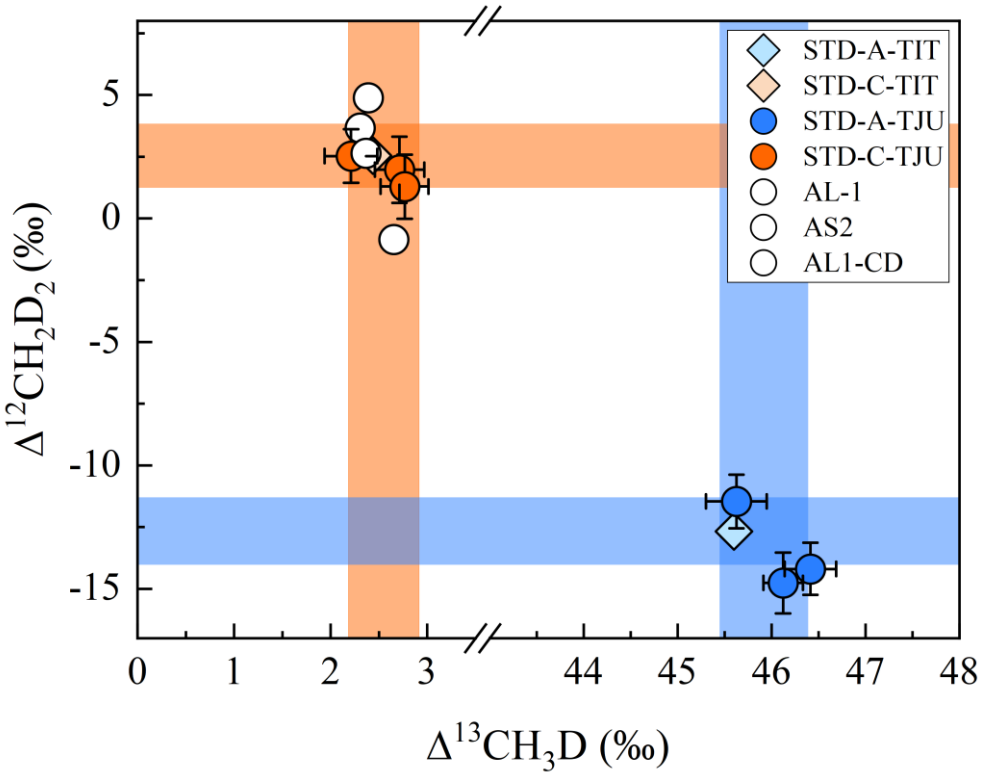

Figure. S12. $\Delta^{13}CH_3D$ v.s. $\Delta^{12}CH_2D_2$ results from inter-laboratory comparisons of the same samples (STD-A and STD-C) measurements . The TIT and TJU represent Tokyo Institute of Technology and Tianjin University Ultra HR-IRMS laboratories. AL- and AS- samples are measured by Nu Panorama IRMS at UCLA (Young et al., 2017) and by TILDAS at MIT(Gonzalez et al., 2019), transferred to STD-C frame for comparison.

4 References

ABBAS H F, WAN DAUD W M A 2010. Hydrogen production by methane decomposition: A review. International Journal of Hydrogen Energy [J], 35: 1160-1190.

ASAI K, NAGAYASU Y, TAKANE K, et al. 2008. Mechanisms of Methane Decomposition over Ni Catalysts at High Temperatures. Journal of the Japan Petroleum Institute [J], 51: 42-49.

DONG G, XIE H, THIAGARAJAN N, et al. 2020. Clumped isotope analysis of methane using HR-IRMS: New insights into origin and formation mechanisms of.

ELDRIDGE D L, KOROL R, LLOYD M K, et al. 2019. Comparison of Experimental vs Theoretical Abundances of 13CH3D and 12CH2D2 for Isotopically Equilibrated Systems from 1 to 500 °C. Acs Earth and Space Chemistry [J].

GONZALEZ Y, NELSON D D, SHORTER J H, et al. 2019. Precise Measurements

of (12)CH2D2 by Tunable Infrared Laser Direct Absorption Spectroscopy. Analytical Chemistry [J], 91: 14967-14974.

HAYES J M 1982. An introduction to isotopic measurements and terminology. Spectr [J], 8: 3-8.

JAUTZY J J, DOUGLAS P M J, XIE H, et al. 2021. CH4 isotopic ordering records ultra-slow hydrocarbon biodegradation in the deep subsurface. Earth and Planetary Science Letters [J], 562: 116841.

STOLPER D A, SESSIONS A L, FERREIRA A A, et al. 2014. Combined 13C–D and D–D clumping in methane: Methods and preliminary results. Geochimica et Cosmochimica Acta [J], 126: 169-191.

YOUNG E D, KOHL I E, LOLLAR B S, et al. 2017. The relative abundances of resolved l2CH2D2 and 13CH3D and mechanisms controlling isotopic bond ordering in abiotic and biotic methane gases. Geochimica et Cosmochimica Acta [J], 203: 235-264.

ZHANG N, SNYDER G T, LIN M, et al. 2021. Doubly substituted isotopologues of methane hydrate (13CH3D and 12CH2D2): implications for methane clumped isotope effects, source apportionments and global hydrate reservoirs. Geochimica et Cosmochimica Acta [J], 315: 127-151.